Composites: Part A 149 (2021) 106484

Contents lists available at ScienceDirect

Composites Part A

journal homepage: www.elsevier.com/locate/compositesa

On the investigation of quasi-static crack resistance of thermoplastic tape layered composites with multiple delaminations: Approaches for quantification

Anastasiia Khudiakova [a], Andreas J. Brunner [b,1], Markus Wolfahrt [a], Thomas Wettemann [c], Damir Godec [d], Gerald Pinter [e,*]

[a] Polymer Competence Center Leoben GmbH, Roseggerstraße 12, 8700 Leoben, Austria
[b] Swiss Federal Laboratories for Materials Science and Technology, Laboratory for Mechanical Systems Engineering, Überlandstrasse 129, 8600 Dübendorf, Switzerland
[c] Chair of Carbon Composites, Technical University of Munich, Boltzmannstraße 15, 85748 Garching, Germany
[d] Faculty of Mechanical Engineering and Naval Architecture, University of Zagreb, Ul. Ivana Lučića 5, 10000 Zagreb, Croatia
[e] Institute of Materials Science and Testing of Polymers, Montanuniversität Leoben, Otto Glöckel-Straße 2/II, 8700 Leoben, Austria

ARTICLE INFO

Keywords:
Laminates
Delamination
Fracture toughness
Automated tape placement (ATP)

ABSTRACT

The present study is devoted to the quantitative characterisation of the interlayer bonding in unidirectional carbon fibre reinforced thermoplastic laminates produced by automated tape placement with in-situ consolidation (ATPisc). Two different manufacturing protocols were applied to produce the laminates that were further characterised using the quasi-static mode I double cantilever beam (DCB) test. Regardless of the manufacturing approach, the laminates exhibited multiple cracking accompanied by fibre bridging during testing, which affected the main mid-plane crack propagation. This effect was examined by comparing the crack length visually measured during testing with both the crack length back-calculated from the compliance and the crack length calculated using the flexural modulus and the compliance. In addition, the investigation of the evolution of the effective flexural modulus E_1 and the damage parameter φ throughout testing was performed for a better understanding of the damage accumulation in the specimens.

1. Introduction

Automated tape placement with in-situ consolidation (ATPisc) is an additive manufacturing (AM) method enabling the production of carbon fibre reinforced (CFR) thermoplastic laminates. In this process, an incoming prepreg tape is heated with, e.g., a diode laser above the melting temperature of the thermoplastic matrix and placed on a mould using a compaction roller. The intimate contact created between the tape and the roller ideally leads to inter-diffusion of the polymer chains across the bond interface followed by material solidification with subsequent cooling [1]. Fast placement speeds (up to 12 m/min [2]) and rapid cooling rates (up to 500 °C/s [3]) applied in ATPisc lead to very short times of the intimate contact as well as to the limited dwell time of the material above the thermoplastic's glass transition temperature T_g, when the polymer chains are mobile and the inter-diffusion occurs across the interfaces. This results in a short healing time that hinders the development of the bonding between the incoming tape and the substrate [4]. In addition, laminates produced by ATPisc suffer from thermal residual stresses, which are caused by a non-uniform shrinkage of the matrix and the fibres upon cooling and also by temperature gradients throughout the laminate thickness as a result of layer-wise manufacturing. Excessive residual stresses lead to laminate curvature, which may cause delamination between the layers [5–8]. Moreover, the interlayer bonding is a potential site for the accumulation of defects such as voids, which deteriorate the interlayer bonding [9,10]. The cooling rate of the thermoplastic composite manufacturing process affects the degree of crystallinity of the matrix, and somewhat lower quasi-static mode II delamination resistance has been observed for CF-PPS with higher matrix crystallinity [11–13]. Comparative experiments on mode I and mode II in CF-PEEK [14] have indicated an analogous behaviour for

* Corresponding author.
E-mail addresses: anastasiia.khudiakova@pccl.at (A. Khudiakova), andreas.brunner@empa.ch (A.J. Brunner), markus.wolfahrt@pccl.at (M. Wolfahrt), thomas.wettemann@tum.de (T. Wettemann), damir.godec@fsb.hr (D. Godec), gerald.pinter@unileoben.ac.at (G. Pinter).
[1] Retired from Empa.

https://doi.org/10.1016/j.compositesa.2021.106484
Received 19 January 2021; Received in revised form 19 April 2021; Accepted 19 May 2021
Available online 24 May 2021

mode I as for mode II. It is hence plausible to assume that mode I delamination resistance also increases with increasing cooling rate for CF-PPS. However, there are additional effects. Taketa et al. [12] noted that residual stresses in CF-PPS do not seem to show a significant dependence on cooling-rate and hence on crystallinity, contrary to other CF-thermoplastic composites. Gao and Kim [14] noted that matrix crystallinity has an effect on matrix ductility and hence on toughness and delamination resistance of CF-PEEK, but that the fibre–matrix adhesion also plays a role in that. Increasing cooling-rate reduces fibre–matrix adhesion and hence an optimum cooling rate would have to be determined balancing ductility and adhesion. There is no quantitative or semi-quantitative estimate on cooling rates for the different laminates in this manuscript available, and hence the discussion of the interplay between the various factors depending on cooling rate (essentially matrix crystallinity, defect types, concentration and sizes, residual stresses and fibre–matrix adhesion) that in the end yield the observed delamination resistance remains qualitative.

The present work investigates the interlayer bonding in unidirectional (UD) CFR polyphenylene sulphide (PPS) laminates produced by ATPisc. Manufacturing of the laminates followed two different design approaches each with two different combinations of tape placement speed and process temperature, respectively. The quasi-static mode I fracture [15] of the laminates was characterised with double cantilever beam (DCB) specimens. Regardless of the manufacturing approach, the mid-plane delamination propagation was accompanied by the formation of multiple interlayer delaminations in addition to fibre bridging during DCB testing. The effect of fibre bridging in UD CFR composites is well-known in literature [16–18], including studies on UD CF/PPS laminates [19,20], while multiple delaminations have been addressed only in few research works [21,22]. These additional damage processes affect the main mid-plane crack propagation and lead to data that could not be reasonably quantified according to the standard data analysis. Hence, an important goal of this study was to find ways to quantitatively characterise the laminate quality. For this purpose, the evolution of the crack length correction factor Δ and the effective flexural modulus was examined throughout the tests. In addition, the damage parameter φ [23] was calculated to characterise the degree of damage at the beginning and the end of testing. The quasi-static delamination resistance was presented using R-curves (resistance curves) with the energy release rate G_I plotted versus both the crack length back-calculated from the machine compliance and the crack length calculated using the flexural modulus independently measured using three-point bending tests. In addition, three-point bending tests were performed to determine a possible change in the flexural modulus of the DCB specimens prior to and after mode I testing. Moreover, thermogravimetric and optical analyses were performed. To the best of the authors' knowledge, such a complex crack propagation behaviour with multi-cracking has not been reported in former studies of ATPisc laminates [6,24–26,11] nor the approach for their characterisation aiming at quantification, making the present work valuable in this field.

2. Experimental

2.1. Materials and laminate manufacturing

The material used in the present study is a continuous carbon fibre reinforced polyphenylene sulphide (CF-PPS) tape (type PPS-CF67-WD495 from Ticona Polymers, Irving, Texas, no longer produced) with a width of 26.4 mm, a thickness of 0.14 mm and a nominal fibre weight fraction of 67%. The UD laminates with 24 layers were manufactured using ATPisc by following two different approaches as illustrated in Fig. 1. The heating source used was a diode laser with a maximal output capacity of 4000 W and the compaction roller pressure was set to 5 bar for all laminates.

According to the first approach, which is called clamping, a picture frame made out of aluminium profiles was installed above the first four layers that were placed on a flat tool (Fig. 1a). The remaining 20 layers were then laid up on each other within the frame. The laminates produced by this method were flat as long as they stayed fixed with the frame on the manufacturing table (Fig. S1a-a''). After removing the frame, as expected, the laminate edges bent upwards. Such a distortion can be attributed to the fact that the bottom layers which have already solidified constrain the shrinkage of the upper layers during their cooling down, leading to parabolic buckling of the laminate [27].

According to the second approach, which is called flipping, the manufacturing process was stopped to flip the laminate after the deposition of every four layers until 24 layers were placed in total (Fig. 1b). The laminate plates produced by the flipping method were nearly flat (Fig. S1b-b''). This can possibly be explained by two reasons. On the one hand, the flipping process leads to a faster laminate cooling with a reduced heat build-up within the laminate, so accumulation of residual stresses did not take place or to a much lesser extent. On the other hand, the residual stresses accumulating during manufacturing within every four layers could be balanced by residual stresses by the following laminate flipping and heat and pressure application.

A polyimide insert film (from Ube Industries, Yamaguchi, Japan)

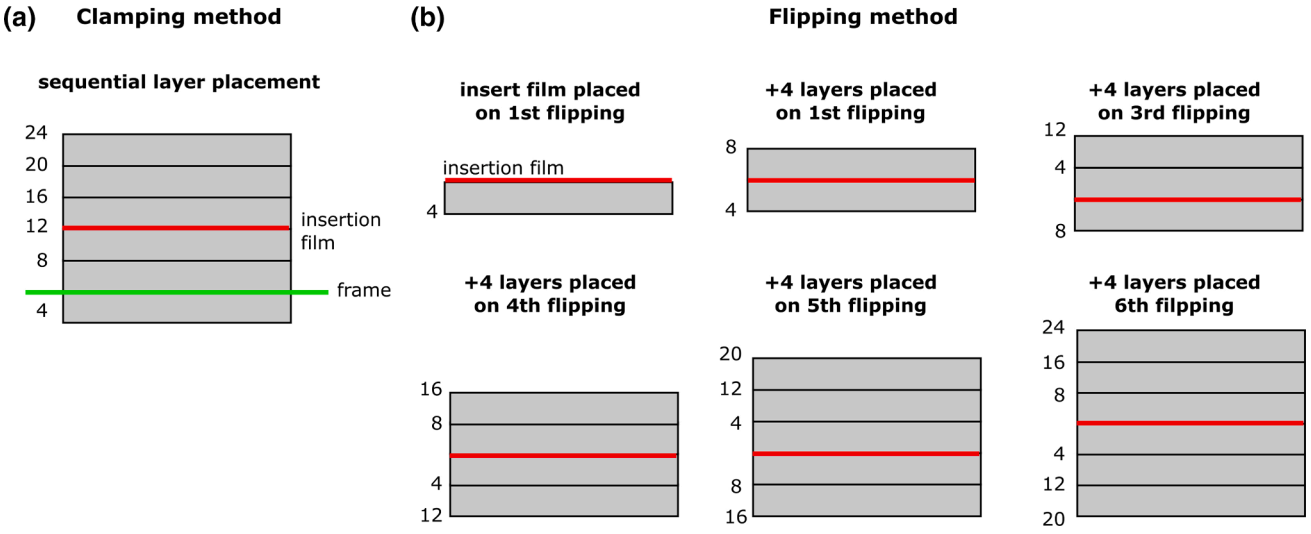

Fig. 1. Schematic drawing of the clamping (a) and the flipping (b) method. The insert film is marked in red, the frame is marked in green. The fibre direction is into the page.

with a thickness of 12.5 μm was placed in the mid-plane of every laminate manufactured to create a pre-crack for delamination testing. To investigate the influence of the placement speed and the process temperature on the fracture toughness, two different sets of manufacturing parameters were chosen. The laminates produced with 5 m/min and 330 °C present the 'slow and cold' case, while the laminates manufactured with 10 m/min and 350 °C present the 'fast and hot' case. The process parameters are listed in Table 1. With respect to the nomenclature of the tests, the letters 'c' and 'f' refer to the manufacturing methods, clamping and flipping. The first number after the letter refers to the placement speed and the second number to the process temperature used. For example, a panel produced at 5 m/min and at 330 °C following the flipping approach is called f-5–330. In c-5–330, residual stresses reached such a high level that transverse cracking of the laminate occurred (Fig. S1a'''). This was not observed for c-10–350. Taketa et al. [12] have indicated that residual stresses in CF-PPS do not depend much on cooling rate. Therefore, the difference in transverse cracking observed is possibly due to the dwell time and/or the placement speed. Assuming that the dwell time at lower temperature would be lower, this may result in less polymer chain interactions and lead to inherently weak adhesion between prepreg layers [28]. On the other hand, the lower placement speed may result in higher energy deposition and the clamping method may favour less energy loss between placing successive prepreg layers. This may then yield higher thermal stresses during final cool-down in case of c-5–330. There was no observable impact of the laminating speed and the process temperature on the laminate curvature for the flipping method.

The laminate curvature observed is expected to affect the beam stiffness and, consequently, the fracture toughness obtained using DCB testing [29]. Yokozeki et al. [30] have examined the effect of thermal residual stresses on the fracture toughness of CF reinforced polymer (CFRP) composites. Finite element modelling (FEM) indicated in this case that the energy release rate is lower when thermal residual stresses are considered. The CFRP was not specified, but the material parameters used for FEM are typical of thermoplastic CFRP, meaning that the effect of residual stresses likely also applies to CF-PPS of the present study.

2.2. Quasi-static mode I DCB testing

Rectangular DCB specimens with dimensions of 150x20x3.2 mm were cut out of the laminates using a waterjet cutting machine. During cutting, another plate placed under the CF/PPS laminates prevented any reflections of the waterjet hitting them. The insert film length was 45 mm. Prior to testing, steel load-blocks were glued to all specimens using a two-component adhesive (type Scotch-weld DP 490 from 3 M, Maplewood, MN, USA). Before gluing, the load-blocks were sanded with a grinding machine and the specimen surface with an abrasive paper and then both were cleaned with isopropanol. After that, the specimens were placed in an oven for 2 h at 65 °C to cure the adhesive. The side surface of the specimens was covered with a thin layer of a white correction fluid to facilitate the visual detection of delamination onset. The tests were performed on an electro-dynamic test machine (type Instron E3000 from Instron, Norwood, MA,USA) equipped with a 250 N load cell (type 2527 Series Dynacell - Dynamic Load Cell ± 250 N from Instron, Norwood, MA, USA). During testing, the load and displacement signals were recorded with a sampling rate of 10 Hz. The tests were performed according to ISO 15024 [15] with a loading speed of 2 mm/min under displacement control. During testing, the crack length a in the mid-plane of the specimen was visually measured using a travelling microscope, while the load and the displacement were recorded by the test machine. Five specimens per laminate were tested 'as received' under standard laboratory conditions (23 °C air temperature, 50% relative humidity).

Table 1
Manufacturing parameters of UD CF/PPS panels produced by ATPisc.

Specimen ID	Manufacturing method	Number of plies	Placement speed, m/min	Process temperature, °C
c-5–330	clamping	24	5	330
c-10–350	clamping	24	10	350
f-5–330	flipping	24	5	330
f-10–350	flipping	24	10	350

During DCB testing, specimens exhibited additional damage processes besides the main mid-plane crack propagation. Fig. 2 demonstrates selected examples of fracture behaviour visually observed during the tests. Most of the specimens yielded pronounced fibre bridging that appeared as a net of fibres pull out of the opened beams (Fig. 2c, d, c', d'). In addition, several specimens showed multiple delamination growth above and/or below the mid-plane (Fig. 2a, b, a', b'). It is further interesting to note that f-5–330-04 and −05 exhibited critical layer delamination due to layer 'buckling' close to the upper surface (Fig. 2c'). Such a type of delamination was not observed for any other specimens in this study. Such a complex delamination behaviour clearly raises the question, how additional damage could possibly be accounted for in the data analysis. It should be noted that despite of multiple delaminations, the force–displacement curves were stable and, in general, the specimens followed linear elastic fracture mechanics (LEFM) behaviour. A typical load–displacement curve is shown in Fig. S2.

2.3. Three-point bending

Pristine specimens and specimens after quasi-static mode I loading were tested using three-point bending to examine the change in flexural modulus E_{1_3pb} before and after testing. The tests were performed on a universal testing machine (type Zwick Z010 from Zwick GmbH & Co. KG, Ulm, Germany) equipped with a load cell of 10 kN in accordance with ASTM D 790 [31]. The loading and support noses both had radii of 5 mm. The span to thickness ratio of 50:1 used for all specimens was chosen as large as possible for the specimen length of 150 mm. The formulas for the loading rates and flexural modulus can be found in the test standard. The flexural tests were performed under standard laboratory conditions on specimens without any conditioning. The pristine specimens refer to additional DCB specimens of the same dimensions of 150x20x3.2 mm that were not tested under quasi-static fracture loading. The specimens after the quasi-static mode I DCB tests were cryo-fractured along the mid-plane, resulting in two individual beams of the same thickness of about 1.6 ± 0.1 mm. After that, these individual beams were tested under three-point bending. Schematic drawings of the three-point bending tests is shown in Fig. S3.

2.4. Optical analysis

In order to investigate the delamination development between the laminate layers, polished cross sections of the specimens were observed using an optical 3D measurement system (type Alicona InfiniteFocus from Alicona Imaging GmbH, Raaba, Austria) prior to and after DCB testing. The sample extraction schematic is illustrated in Fig. 3.

2.5. Thermogravimetric analysis

The fibre weight fraction w_f of the laminates was determined by the thermogravimetric analysis (TGA) (see the Supplementary Information for details). w_f was further used to calculate the fibre volume fraction f_v according to Eq. (1) [32].

$$f_v = \frac{w_f/\rho_f}{\frac{w_f}{\rho_f} + \frac{1-w_f}{\rho_m}} \quad (1)$$

where ρ_f, ρ_m are the densities of the fibre and matrix, respectively.

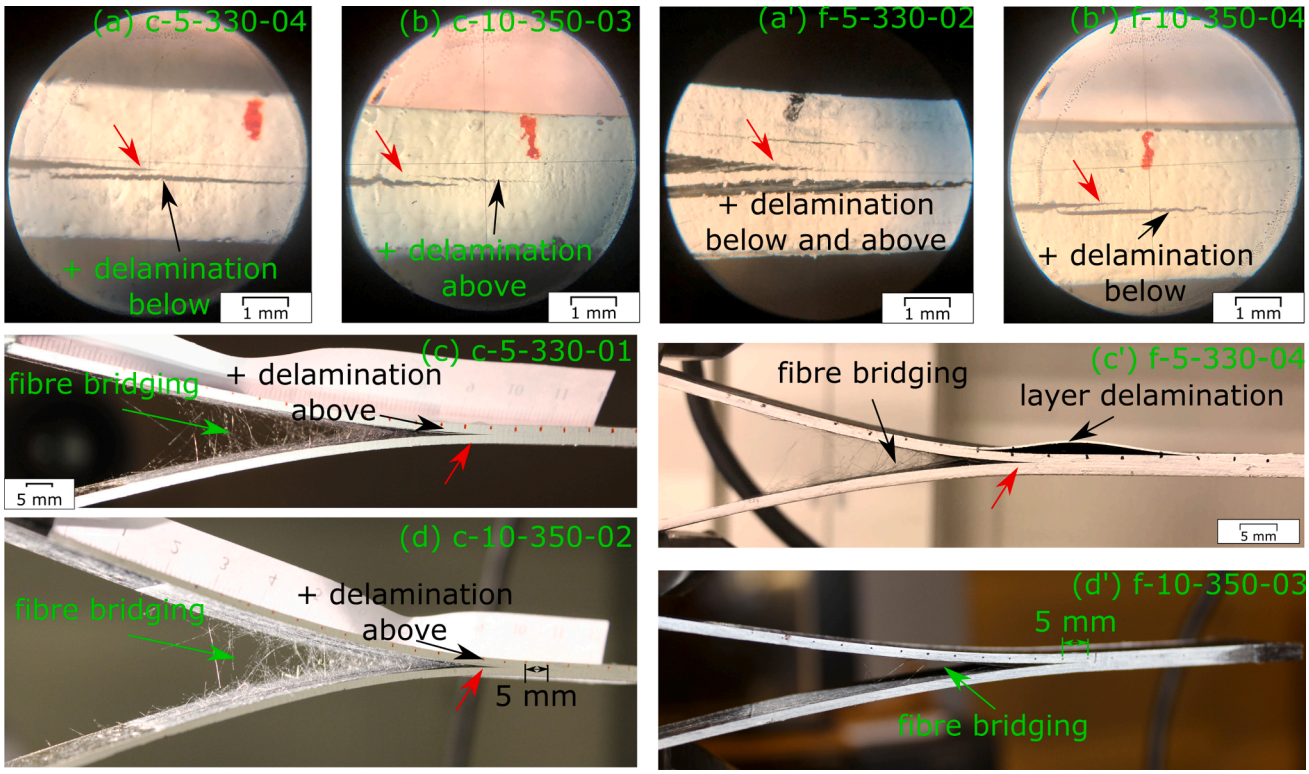

Fig. 2. Selected examples of crack growth and fibre bridging in laminates produced by clamping (a-d) and flipping (a'-d') methods. The total crack length was about 60 mm in (a), 85 mm in (b), 60 mm in (a') and 55 mm in (b'). The red arrows point to the mid-plane delamination. Photos a, a', b, b' are side views made though a travelling microscope. The direction of the crack propagation is from left to right in all photos.

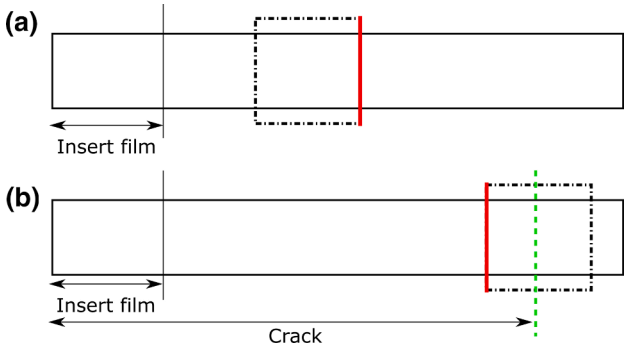

Fig. 3. Schematic illustrations of the samples extracted out of the DCB specimens for the microscopic examinations: pristine specimens (a) and specimens after quasi-static testing (b). The view is on the top specimen surfaces. The green dashed line refers to the final crack tip after DCB testing (b). The black dot-dashed lines refer to the samples cut out of the DCB specimens, with the surfaces examined using the optical microscope marked in red. The figure is not scaled.

3. Data analysis techniques

3.1. Crack length correction factor Δ and effective flexural modulus E_1

The data analysis was started with the calculations of the crack length correction factor Δ, which is required for calculations of both the damage parameter φ [23,33] and the strain energy release rate using corrected beam theory [15]. The crack length correction factor Δ was determined by plotting the cube root of the corrected compliance $(C/N_{block})^{1/3}$ versus crack length a, where the latter was defined in three different ways. The crack length was taken to be equivalent to (i) a_m measured visually with a travelling microscope during testing, (ii) a_{calc} back-calculated from the compliance using Eq. (3), and (iii) a_{eff} calculated using the effective crack length method (ECLM, Eq. (4)). The compliance was calculated as displacement divided by load automatically recorded by the test machine during tests. The compliance calibration enables calculation of the crack length taking into account changing of the specimen compliance C that was automatically measured by the test machine [34]. Whereas ECLM enables calculations of the effective crack length a_{eff} using C and an independently measured flexural modulus E_1, and accounts for the fracture process zone and associated crack tip effects [35]. Δ is defined as the absolute value of the intersection of the linear regression fitted to the data with the negative X-axis (Eq. (2)). Δ is set to zero in case of a positive intercept [15].

$$(C/N_{block})^{1/3} = A_0 + A_1 a, \Delta = -\frac{A_0}{A_1} \tag{2}$$

where C is the compliance, N_{block} is the load block correction, A_0 and A_1 are parameters of the linear fit.

$$C = D^* a^m \tag{3}$$

where D is a constant and m is the exponent of the power law.

$$a_{eff} = \frac{h}{2}\left(\frac{E_1 bC}{N_{block}}\right)^{1/3} \tag{4}$$

where h is the thickness of one beam, b is the specimen width, E_1 is the flexural modulus. For analysis of every fractured specimen, a value of E_1 was taken to be equivalent to E_{1_3pb} obtained from a three-point bending test performed on these specimen beams after DCB testing. In addition, the effective flexural modulus E_1 was calculated at each data point for every specimen using Eq. (5) [35].

$$E_1 = \frac{8N_{block}(a + |\Delta|)^3}{Cbh^3} \tag{5}$$

3.2. Damage parameter φ

In order to estimate the degree of damage, the damage parameter φ was used and deduced via Eq. 6 and 7 [23,33]. φ characterises the damage at the crack tip caused by micro-cracking. It has a value in a range between 0 and 1 meaning the total loss of shear and transverse stiffness for $\varphi = 0$ and the absence of damage for $\varphi = 1$.The latter means that Δ takes on a value of $\Delta_{elastic}$ in Eq. (6) written for an anisotropic composite, where the first term is the contribution from the shear deformation and the second from the transverse deformation [33]. More details can be found in [36].

$$\chi^2 = \left(\frac{\Delta}{h}\right)^2 = \frac{1}{10}\left(\frac{E_1}{\varphi G_{12}} - 2\vartheta\right) + 0.24\sqrt{\frac{E_1}{\varphi E_2}} \tag{6}$$

$$\varphi = \left(\frac{0.12}{\chi^2+0.06}\sqrt{\frac{E_1}{E_2}}\left(1+\sqrt{1+7(\chi^2+0.06)\frac{E_2}{G_{12}}}\right)\right)^2 \text{ for} \vartheta = 0.3 \tag{7}$$

where E_2 is the transverse modulus, G_{12} is the out-of-plane shear modulus and ϑ is the Poisson's ratio. The calculations of φ for every specimen were performed using the corresponding flexural modulus E_{1_3pb} obtained using a three-point bending test. E_2 and G_{12} were determined using the Reuss model for each laminate type (see the calculations in the Supplementary Information for details).

3.3. Calculations of G_I

The mode I energy release rate (ERR), G_I, was calculated according to either corrected beam theory (CBT) (Eq. (8), [15]) or ECLM (Eq. (9), [35]).

$$G_I = \frac{3P\delta}{2b(a+|\Delta|)}\frac{F_{displ}}{N_{block}}$$
$$F_{displ} = 1 - \frac{3}{10}\left(\frac{\delta}{a}\right)^2 - \frac{3}{2}\left(\frac{\delta l_1}{a^2}\right) \tag{8}$$
$$N_{block} = 1 - \left(\frac{l_2}{a}\right)^3 - \frac{9}{8}\left[1 - \left(\frac{l_2}{a}\right)^2\right]\frac{\delta l_1}{a^2} - \frac{9}{35}\left(\frac{\delta}{a}\right)^2$$

$$G_I = \frac{3P\delta}{2ba_{eff}}\frac{F_{displ}}{N_{block}} \tag{9}$$

where P is the applied load, δ is the displacement, F_{displ} is the large-displacement correction, l_1 is the distance between the center of loading pin to the mid-plane of the half-beam of the DCB specimen, l_2 is the distance between the centre of the loading pin to the edge of load block. G_I was calculated for every value of the crack length a and corresponding P and δ. The data obtained was presented using R-curves.

4. Results and discussion

4.1. Thermogravimetric analysis

The results of specific fibre weight fraction w_f values are summarised in Table 2. The corresponding fibre volume fractions f_v were calculated using Eq. (1) with fibre density ρ_f of 1.8 g/cm^3 and PPS density ρ_m of 1.35 g/cm^3 [37]. It should be noted that f_v obtained was further used for the calculations of both the transverse and shear moduli (see the equations in the Supplementary Information for details).

Table 2
Fibre weight and volume fractions of the laminates obtained using TGA analysis. m corresponds to the sample weight before the TGA.

Laminate	m, mg	w_f, %	f_v, %
c-5–330	20.8 ± 0.1	64.7 ± 2.0	57.9 ± 0.2
c-10–350	20.0 ± 0.6	60.6 ± 1.7	53.6 ± 1.7
f-5–330	20.3 ± 0.6	58.7 ± 0.9	51.6 ± 1.0
f-10–350	20.0 ± 0.4	67.1 ± 0.8	60.4 ± 0.9

4.2. Optical analysis

The micrographs of the laminate cross sections made after DCB testing are shown in Fig. 4. It was revealed that although only one mid-plane delamination was visually observed on the side specimen surface during testing, other damage processes have also occurred in the specimen body. For example, only one mid-plane delamination was visually observed during testing c-5–330-01. However, its micrograph showed the presence of transverse intralaminar cracking that provoked extra delamination growth above and below the mid-plane (Fig. 4a). Such a transverse cracking was also observed in the micrographs of the pristine c-5–330 specimen, which was caused by excessive thermal residual stresses (Fig. S4a). Similarly, for c-10–350-01 the main crack did not propagate only in the mid-plane, but it deviated from it to the adjacent layers (Fig. 4b). The micrograph of f-10–350-05 with a single delamination observed during testing also revealed the presence of crack branching out of the mid-plane to adjacent layers. Layer misalignments, porosity and non-uniform fibre distribution can also be seen in the micrographs made prior and after DCB testing (Fig. S4, Fig. 4). The optical analysis also revealed the presence of multiple interlayer delamination in f-5–330 prior to and after testing, which were not observed in other laminate types (Fig. S4b, Fig. 4b). This could mean that process parameters of 5 m/min and 330 °C did not provide the heat to sufficiently melt the substrate. On the other hand, multiple delaminations could partially or fully be an artefact from cutting and preparing of the laminate cross-sections, but would still reflect local weak interlayer bonding.

4.3. Three-point bending tests

Table 3 shows the results of three-point bending tests performed on the pristine specimens and the specimens after DCB testing. There was no significant difference found between their E_{1_3pb}. All flexural moduli of the pristine specimens exhibited the standard deviation within 5% of the respective average. This indicates reasonable and consistent, but not excellent, quality of the laminates. The scatter after DCB testing is the same, except for f-5–330 type specimens. The absence of a pronounced change in the modulus values determined before and after testing on one hand may be interpreted that most of damage that affects the flexural modulus was already induced in the laminates during their manufacturing (Fig. S4). On the other hand, these findings may be due to the effect that the three-point bending modulus is not sufficiently sensitive to delaminations in the beam. Compression and shear may 'close' some of the delaminations present and hence 'hide' damage created during the fracture tests.

4.4. DCB testing

4.4.1. Crack length correction factor Δ for a_m, a_{calc} and a_{eff}

To obtain the crack length correction factor Δ, $(C/N_{block})^{1/3}$ was plotted versus the crack length a equivalent to (i) a_m visually measured during testing, (ii) a_{calc} calculated using Eq. (3), and (iii) a_{eff} calculated using Eq. (4) (Fig. 5a, Fig. S5). In order to check the linearity of the data obtained, linear regressions were fitted to every dataset out of five consecutive points (Fig. 5b, Fig. S6). It was found that $(C/N_{block})^{1/3}$ plotted versus a_m highly deviates from linearity for all specimens, yielding the fact that Δ highly depends on the number of points fitted to the linear regression. Such a deviation from linearity suggests that the visual crack length measurements were affected by additional damage processes that could not be observed visually on the specimen side surface. It is also possible that part of this variation could be due to the fact that the crack length was erroneously measured by the machine operator, e.g. caused by limited visibility or subjective interpretation of

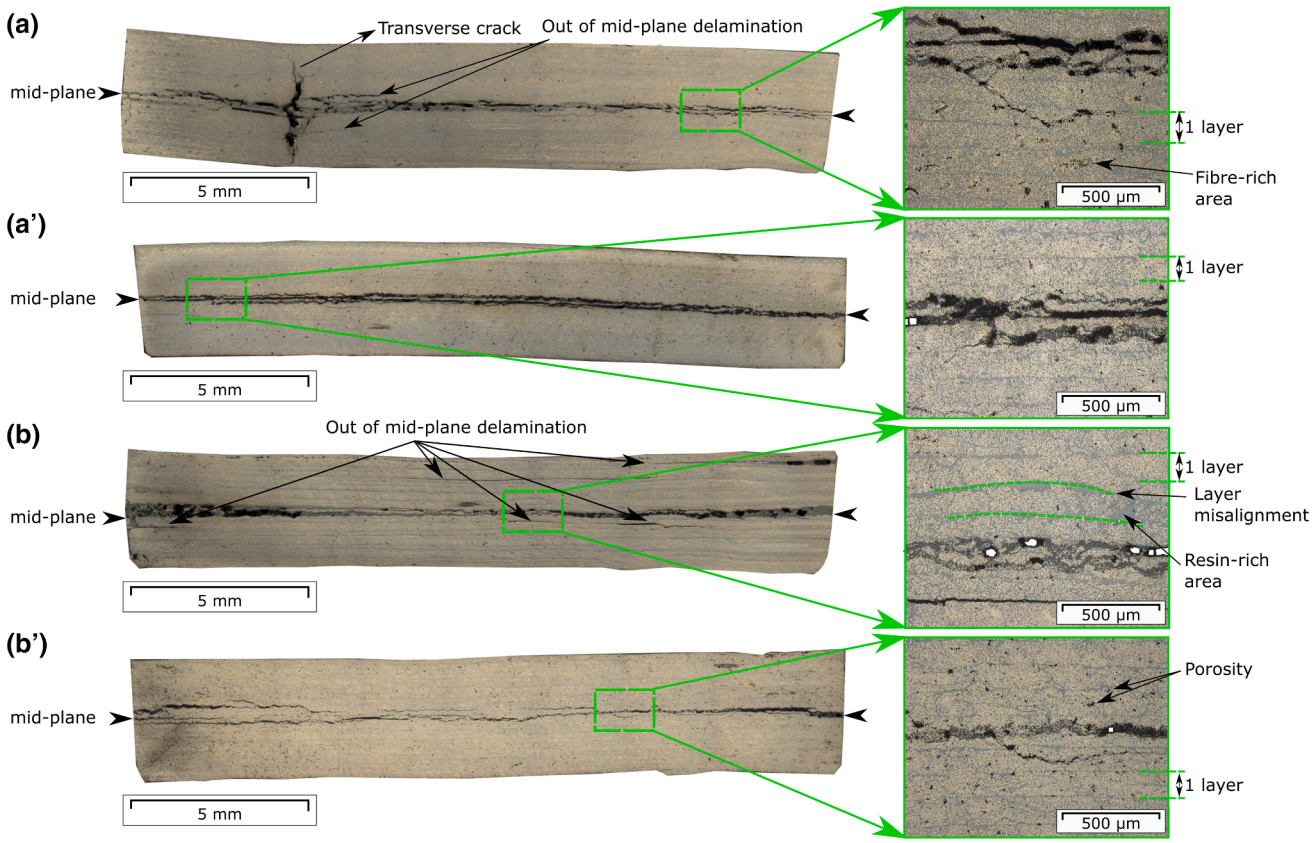

Fig. 4. Micrographs of the polished cross sections of selected laminates made after quasi-static mode I DCB testing for c-5–330-01 (a), c-10–350-01 (a'), f-5–330-04 (b) and f-10–350-05 (b').

Table 3
The flexural moduli obtained from three-point bending tests performed on pristine specimens and specimens after quasi-static mode I DCB testing. The values presented were calculated as the arithmetic mean of four pristine specimens for c-5-330; of five pristine specimens for c-10-350, f-5-330 and f-10-350; of four specimens tested under quasi-static mode I loading for every laminate type.

Laminate	E_{1_3pb}, GPa	
	Pristine specimens	After DCB testing
c-5–330	111 ± 6 (6%)	111 ± 5 (5%)
c-10–350	96 ± 4 (4%)	95 ± 5 (5%)
f-5–330	104 ± 3 (3%)	100 ± 15 (15%)
f-10–350	112 ± 8 (7%)	112 ± 6 (5%)

observed features [38]. Micro-cracking and fibre bridging at the crack tip, for example, made the measurements of the crack length particularly difficult. In addition, there could be inaccuracies of the visual crack length measurement caused by the crack front curvature [23]. Thus, this undermines the use of visually measured crack length for further calculations. For the calculated crack length data, the slopes of the linear regressions either continuously increased, decreased or stayed stable with the crack growth. The increasing slopes can be explained by the development of additional damage processes occurring during testing, which effectively reduces the specimen stiffness and hence increases the slope of the fit [23]. Thus, the back-calculated data yielded more consistent results than the visually measured data. The back-calculated data would take all damage created into account, however, somehow weighted by where this damage was located. In Ref. [39], it was shown that both length and locations of multiple delaminations have an influence on the strain energy release rate. The slopes of the effective crack length data stayed constant with the crack growth due to the linear relationship between $(C/N_{block})^{1/3}$ and a_{eff} as follows from Eq. (4).

4.4.2. *Effective flexural modulus E_1 and damage parameter φ for a_{calc}*

In order to examine the changing stiffness during DCB testing, the effective flexural moduli E_1 were calculated (Eq. (5)) at the beginning and the end of testing using the calculated crack length data. For this purpose, linear regressions were fitted to the data range of the first and last 25 mm of the crack increment, yielding corresponding Δ_{start} and Δ_{end} (Table S2). For comparison, a linear regression was also fitted to all data points. The results of E_1 obtained are summarised in Table 4. All specimens of c-5–330 and f-10–350 with $\Delta < 0$, showedE_{1start} smaller than E_{1end}. This effect can be explained by fibre bridging developed at the crack tip, which increases the effective stiffness of the DCB specimen [40]. For almost all specimens of c-10–350 and f-5–330 with $\Delta < 0$, the Δ-values were nearly the same at the start, end and throughout the entire data range, resulting in nearly constant E_1. Clearly, the specimens, for which a zero value of Δ was used, yielded a constant value of E_1. The absolute values of Δ and E_1 obtained on the entire data range were in a range between $|\Delta|_{start}$ and $|\Delta|_{end}$ and E_{1start} and E_{1end} for every specimen with $\Delta < 0$. Interestingly, the average effective flexural modulus $E_{1allpoints}$ for c-5-330 and f-10-350 were 1.6 and 1.1 times higher than the corresponding E_{13pb} obtained using three-point bending tests (Table 3). While the average $E_{1allpoints}$ for c-10-350 and f-5-330 correlated fairly well with the corresponding E_{1_3pb}. The higher E_1 obtained from DCB tests has been also reported in [23], where it was attributed to the fibre bridging effect. It has also been noted there that E_1 obtained in DCB tests should not be quoted as the flexural modulus of the laminates due to this discrepancy.

Further, Δ_{start} andΔ_{end} were used for calculations of χ_{start}, χ_{end} (Table S3) and φ_{start}, φ_{end} to characterise the degree of damage. The results of φ obtained are presented in Table 5. All c-5-330 specimens

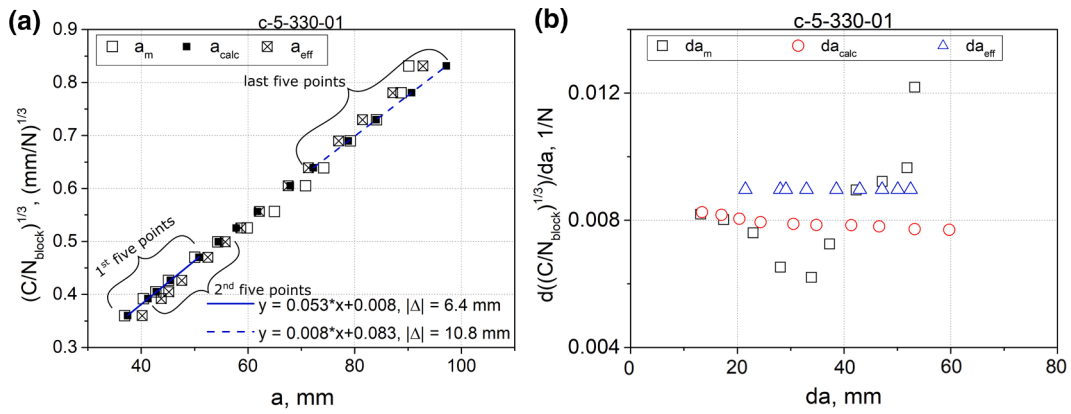

Fig. 5. Plots of $(C/N_{block})^{1/3}$ versus a, where a is either a_m, a_{calc}, or a_{eff} (a) and the values of the slopes of linear regressions, which were fitted to datasets of five consecutive points from the start to the end of the test (b) for c-5–330-01 as a representative example of the data evaluation performed. The plots for all specimens can be found in the Supplementary Information (Fig. S5 and S6).

Table 4
Effective flexural modulus E_1 calculated at the first and last 25 mm of the crack increment and at the entire range of the crack length (E_{1start}, E_{1end} and $E_{1allpoints}$,).

Clamping							
5-330				**10-350**			
Specimen	E_{1start}, GPa	E_{1end}, GPa	$E_{1allpoints}$, GPa	**Specimen**	E_{1start}, GPa	E_{1end}, GPa	$E_{1allpoints}$, GPa
01*	153 ± 12	173 ± 14	163 ± 13	**01***	101 ± 3	101 ± 3	101 ± 3
02*	154 ± 18	193 ± 25	171 ± 20	**02**	101 ± 3	108 ± 4	104 ± 3
03	149 ± 11	163 ± 12	154 ± 11	**03**	87 ± 6	87 ± 6	87 ± 6
04	133 ± 8	160 ± 10	148 ± 8	**04**	103 ± 3	101 ± 3	102 ± 3
05*	222 ± 34	348 ± 61	269 ± 42	**05***	106 ± 6	106 ± 6	106 ± 6
Flipping							
5-330				**10-350**			
Specimen	E_{1start}, GPa	E_{1end}, GPa	$E_{1allpoints}$, GPa	**Specimen**	E_{1start}, GPa	E_{1end}, GPa	$E_{1allpoints}$, GPa
01*	99 ± 8	99 ± 8	99 ± 8	**01**	136 ± 6	136 ± 6	136 ± 6
02	74 ± 5	74 ± 5	74 ± 5	**02**	139 ± 17	138 ± 16	142 ± 17
03	165 ± 22	184 ± 25	173 ± 23	**03***	128 ± 3	143 ± 5	133 ± 3
04	75 ± 3	72 ± 3	74 ± 3	**04**	110 ± 12	110 ± 12	110 ± 12
05	114 ± 4	123 ± 5	118 ± 4	**05***	100 ± 4	116 ± 6	107 ± 4

* A single mid-plane delamination was observed visually on the specimen surface during testing

Table 5
Damage parameter φ calculated at the first and last 25 mm of the crack increment and at the entire range of the crack length (φ_{start}, φ_{end} and $\varphi_{allpoints}$,).

Clamping							
5-330				**10-350**			
Specimen	φ_{start}	φ_{end}	$\varphi_{allpoints}$	**Specimen**	φ_{start}	φ_{end}	$\varphi_{allpoints}$
01*	0.266	0.138	0.182	**01***	5.225	6.083	5.688
02*	0.180	0.067	0.107	**02**	2.470	0.908	1.582
03	0.765	0.358	0.565	**03**	368.749	368.749	368.749
04	0.274	0.120	0.166	**04**	11.786	20.580	16.313
05*	0.037	0.013	0.022	**05***	1.902	1.836	1.860
Flipping							
5-330				**10-350**			
Specimen	φ_{start}	φ_{end}	$\varphi_{allpoints}$	**Specimen**	φ_{start}	φ_{end}	$\varphi_{allpoints}$
01*	332.410	332.410	332.410	**01**	416.757	416.757	416.757
02	471.264	471.264	471.264	**02**	39.986	11.271	24.090
03	0.624	0.145	0.183	**03***	0.623	0.246	0.418
04	21.595	11.846	74.291	**04**	442.804	442.804	442.804
05	0.839	0.419	0.576	**05***	0.698	0.225	0.383

* a single mid-plane delamination was observed visually on the specimen surface during testing

exhibited φ in a range between 0 and 1, while none of c-10-350 specimens showed φ in this range, except c-10-350-02 with φ_{end} of 0.908. For both f-5-330 and f-10-350, two out of five specimens yielded physically acceptable values of φ. In order for φ to be in a range between 0 and 1, $|\Delta|$ should be greater than $|\Delta|_{elastic}$, which was estimated to be of about 3.7 mm (Eq. (6) with $\varphi = 1$). Additionally, it can be derived from Eq. (6) that χ^2 smaller than 5.23 yields values of φ higher than 1. This corresponds to too steep slopes of $(C/N_{block})^{1/3}$ plotted versus crack length a, where the intercept is at a positive crack length value. For φ in a range between 0 and 1, φ_{end} was smaller than φ_{start}, indicating a larger extent of damage at the end of testing. The damage parameters obtained correlate well with the extent of damage observed in the micrographs of the specimen cross sections. For example, more damage can be observed in the cross-section of c-5-330-01 (Fig. 4a) in comparison with the cross-section of f-10-350-05 (Fig. 4b'). This agrees with their damage parameters, which are smaller for c-5-330-01 than for f-10-350-05 (Table 5).

4.4.3. R-curves for a_{calc} and a_{eff}

G_{Ic} was calculated using both CBT with a_{calc} (Eq. (8)) and ECLM with a_{eff} (Eq. (9)). In CBT, the crack length correction factor $\Delta_{allpoints}$ was used as a value in a range between Δ_{start} and Δ_{end} (Table S2). The comparison of the R-curves obtained are presented in Fig. 6. R-curves of clamping-laminates exhibited a better correlation with each other within one parameter set than those of flipping-laminates. The higher repeatability of the results shown by clamping-laminates indicates that this method yields specimens with more consistent properties than the flipping method. R-curves of both clamping and flipping-laminates obtained using ECLM showed less scatter than those obtained using CBT. Thus, the comparison of fracture behaviours was based on the effective data. The $G_{Ic\_initiation}$ values were determined from the initial load–displacement curves using the '5%/MAX point' method described in [15]. $G_{Ic\_propagation}$ was defined as the arithmetic mean of the points on the plateau regions between 50 and 80 mm. The results of $G_{Ic\_initiation}$ and $G_{Ic\_propagation}$ are summarised in Table 6.

Both $G_{Ic\_initiation}$ and $G_{Ic\_propagation}$ obtained for c-10–350 were higher than for c-5–330. The observed increase in fracture toughness might be explained by being a result of both higher temperature and faster placement speed applied. The higher temperature yielded longer dwell

Table 6
$G_{Ic\_initiation}$ and $G_{Ic\_propagation}$ of the DCB specimens.

Laminate	$G_{Ic\_initiation}$, J/m^2	$G_{Ic\_propagation}$, J/m^2
c-5–330	128 ± 16 (12%)	1234 ± 101 (8%)
c-10–350	245 ± 25 (10%)	1635 ± 85 (5%)
f-5–330	173 ± 44 (26%)	1250 ± 220 (18%)
f-10–350	112 ± 41 (36%)	1096 ± 228 (21%)

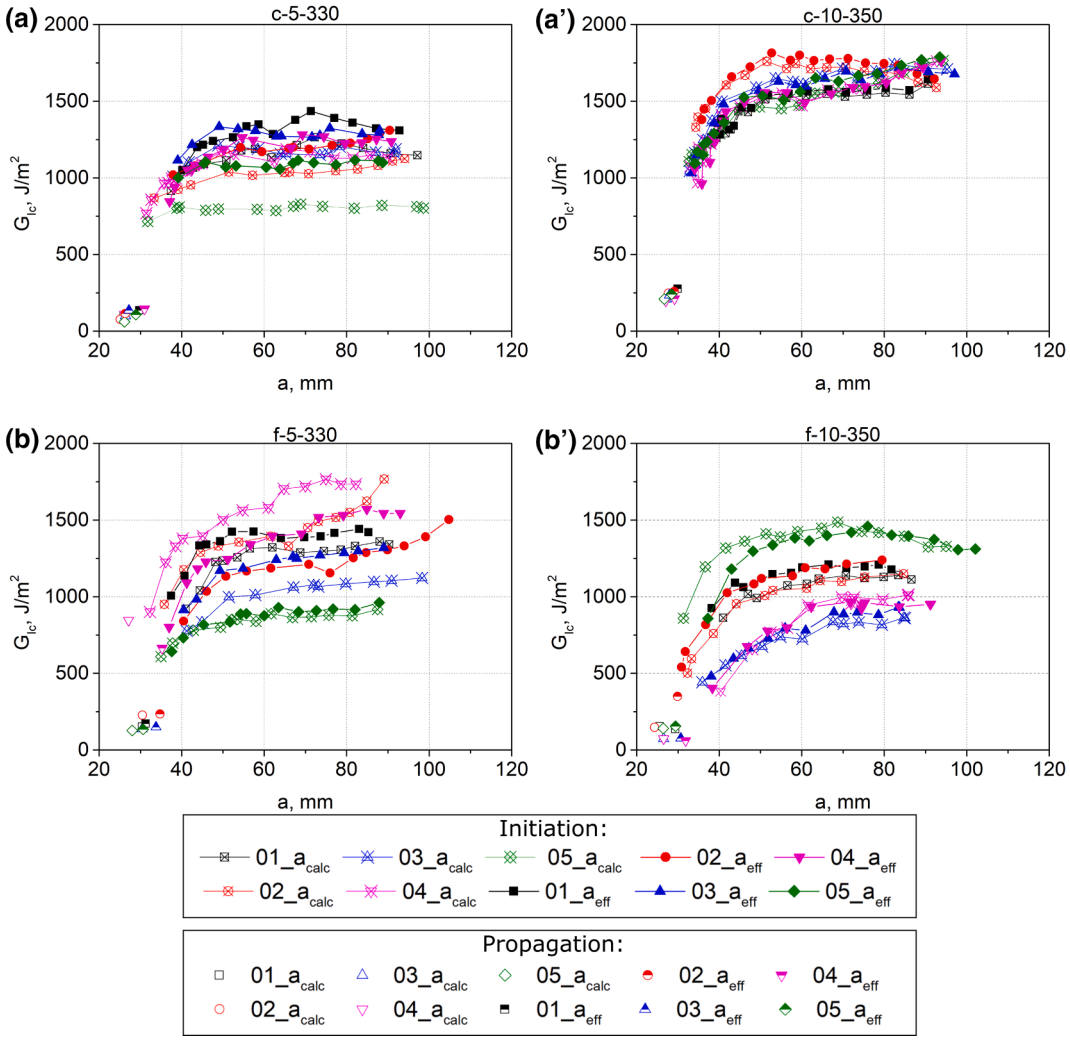

Fig. 6. R-curves for c-5–330 (a), c-10–350 (a'), f-5–330 (b) and f-10–350 (b'), where G_{Ic} was calculated using either CBT with a_{calc} or ECM with a_{eff}. The legends refer to every plot.

time of the laminate above T_g of the matrix, which favoured the better inter-diffusion of the polymer chains [1]. The faster placement speed led to the faster building process and less temperature fluctuations within the laminate, so laminates c-10–350 had a more stable thermal history. For the flipping-method, higher G_{Ic} was demonstrated by the laminates produced with slower speed and lower temperatures. This could probably imply that the heat accumulation did not take place in the flipping method due to multiple process interruptions made to flip the laminate. Thus, the use of higher temperatures did not result in better adhesion between the layers. For most of c-10–350 and f-5–330 specimens, R-curves rise with increasing crack growth. Usually such a behaviour is explained by fibre bridging and/or multiple cracking occurring in specimens, which lead to increasing G_{Ic} [41]. In general, the laminates exhibiting a multiple cracking are expecting to show higher G_{Ic} than if they would not have this effect. This is due to the fact that multiple cracking causes additional energy released per newly fractured surfaces. In addition, the multiple cracking can cause secondary fracture modes, which also increase G_{Ic} [22]. The second factor contributing to the overestimation of G_{Ic} is the fibre bridging that significantly slows down the main crack propagation [42]. This would mean that the results obtained here overestimate the real G_{Ic} value of CF/PPS material without fibre bridging and multiple cracking.

The results showed by c-5-330, f-5-330 and f-10-350 correlate fairly well with $G_{Ic\_propagation}$ reported for press-consolidated UD CF/PPS laminates in Ref.[11]; of 1100 ± 110 J/m^2. Whereas $G_{Ic\_propagation}$ of c-10–350 was 48% higher. In Ref. [11], it was demonstrated that the fracture toughness depends on the degree of crystallinity, which in turn depends on the cooling rate. Therefore, the disturbance in G_{Ic} could also be caused by different degrees of crystallinity.

5. Conclusion

The present study deals with the problem of interlayer bonding in unidirectional CF/PPS laminates produced by automated tape placement with in-situ consolidation (ATPisc). The laminates were produced following two different manufacturing protocols, resulting in different laminate quality. During quasi-static mode I DCB testing performed, the laminate specimens exhibited multiple delaminations growth besides the main mid-plane propagation. The damage accumulation throughout the tests was characterised by means of the damage parameter φ [23]. The cube root of the corrected compliance plotted versus a_m was found to highly deviate from linearity, yielding evidence for the influence of damage processes on the main mid-plane crack growth. This led to uncertainties as to which value of the crack length correction factor Δ should be used to calculate G_I according to the corrected beam theory. Therefore, the quasi-static delamination resistance was characterised using R-curves with a_{calc} back-calculated using the compliance automatically measured by the test machine and a_{eff} calculated using the flexural modulus independently measured and the compliance; they both yielded more consistent results than the visually measured data. Further, R-curves of the effective crack length data showed less scatter than those of the back-calculated crack length data. Therefore, the effective crack length method can be recommended to quantify multiple delaminations, since a_{eff} incorporates all damage in the DCB beam that occurs during testing, independent of its location. Three-point bending tests were employed to identify whether the damage effects led to a change in flexural modulus, but these turned out to be not sensitive enough. Moreover, a microscopic analysis of the laminate cross-sections was performed to examine damage in the specimens prior to and after DCB testing revealing extensive multiple cracks that were not always observable on the edge of the DCB specimens.

Future research will focus on the characterisation of the fatigue delamination resistance of the ATPisc laminates presented here. Research into solving the problem of multiple delaminations and accounting them in the data analysis of the fatigue behaviour is already underway.

CRediT authorship contribution statement

Anastasiia Khudiakova: Conceptualization, Investigation, Formal analysis, Validation, Writing - original draft, Writing - review & editing. **Andreas J. Brunner:** Conceptualization, Validation, Writing - review & editing. **Markus Wolfahrt:** Supervision, Project administration. **Thomas Wettemann:** Resources. **Damir Godec:** Supervision. **Gerald Pinter:** Conceptualization, Supervision, Writing - review & editing.

Declaration of Competing Interest

The authors declare that they have no known competing financial interests or personal relationships that could have appeared to influence the work reported in this paper.

Acknowledgments

The research work was performed within the COMET project VI-2.06, 'New strategies towards laser assisted manufacturing of fibre reinforced thermoplastic composites,' at the Polymer Competence Center Leoben GmbH (PCCL, Austria) within the framework of the COMET program of the Federal Ministry for Transport, Innovation and Technology and the Federal Ministry of Science, Research and Economy with contributions by Technical University of Munich (Institute for Carbon Composites), Montanuniversitaet Leoben (Institute of Material Science and Testing of Polymers), AFPT and Cevotec. The PCCL is funded by the Austrian Government and the State Governments of Styria, Lower Austria and Upper Austria. Special thanks go to Sebastian Maar and Franz Grassegger for their assistance with the specimen preparations.

Appendix A. Supplementary material

Supplementary data to this article can be found online at https://doi.org/10.1016/j.compositesa.2021.106484.

References

[1] Grouve WJB, Warnet LL, Rietman B, Visser HA, Akkerman R. Optimization of the tape placement process parameters for carbon–PPS composites. Compos Part A Appl Sci Manuf 2013;50:44–53.
[2] Comer AJ, Ray D, Obande WO, Jones D, Lyons J, Rosca I, et al. Mechanical characterisation of carbon fibre–PEEK manufactured by laser-assisted automated-tape-placement and autoclave. Compos Part A Appl Sci Manuf 2015;69:10–20.
[3] Stokes-Griffin CM, Compston P. Investigation of sub-melt temperature bonding of carbon-fibre/PEEK in an automated laser tape placement process. Compos Part A Appl Sci Manuf 2016;84:17–25.
[4] Stokes-Griffin CM, Compston P. The effect of processing temperature and placement rate on the short beam strength of carbon fibre–PEEK manufactured using a laser tape placement process. Compos Part A Appl Sci Manuf 2015;78:274–83.
[5] Adams ME, Campbell GA, Cohen A. Thermal stress induced damage in a thermoplastic matrix material for advanced composites. Polym Eng Sci 1991;31(18):1337–43.
[6] Ray D, Comer AJ, Lyons J, Obande W, Jones D, Higgins RMO, et al. Fracture toughness of carbon fiber/polyether ether ketone composites manufactured by autoclave and laser-assisted automated tape placement. J Appl Polym Sci 2014;132(11).
[7] Zhang Y, Xia Z, Ellyin F. Evolution and influence of residual stresses/strains of fiber reinforced laminates. Compos Sci Technol 2004;64(10–11):1613–21.
[8] Gillespie JW, Chapman TJ. The Influence of Residual Stresses on Mode I Interlaminar Fracture of Thermoplastic Composites. J Thermoplast Compos Mater 1993;6(2):160–74.
[9] Khan MA, Mitschang P, Schledjewski R. Parametric study on processing parameters and resulting part quality through thermoplastic tape placement process. J Compos Mater 2013;47(4):485–99.
[10] Pitchumani R, Ranganathan S, Don RC, Gillespie Jr JW, Lamontia MA. Analysis of transport phenomena governing interfacial bonding and void dynamics during thermoplastic tow-placement. Int J Heat Mass Transf 1996;39(9):1883–97.
[11] Sacchetti F, Grouve WJB, Warnet LL, Villegas IF. Effect of cooling rate on the interlaminar fracture toughness of unidirectional Carbon/PPS laminates. Eng Fract Mech 2018;203:126–36.

[12] Taketa I, Kalinka G, Gorbatikh L, Lomov SV, Verpoest I. Influence of cooling rate on the properties of carbon fiber unidirectional composites with polypropylene, polyamide 6, and polyphenylene sulfide matrices. Adv Compos Mater 2020;29(1):101–13.
[13] Lona Batista N, Anagnostopoulos K, Cocchieri Botelho E, Kim H. Influence of crystallinity on interlaminar fracture toughness and impact properties of polyphenylene sulfide/carbon fiber laminates. Eng Fail Anal 2021;119:104976.
[14] Gao S-L, Kim J-K. Cooling rate influences in carbon fibre/PEEK composites. Part II: Interlaminar fracture toughness. Compos Part A Appl Sci Manuf 2001;32(6):763–74.
[15] ISO 15024: 2001 Fibre-reinforced Plastic Composites: Determination of Mode I Interlaminar Fracture Toughness, GIC, for Unidirectionally Reinforced Materials.
[16] Hashemi S, Kinloch AJ, Williams JG. The Analysis of Interlaminar Fracture in Uniaxial Fibre-Polymer Composites. Proc R Soc Lond 1872;1990(427):173–99.
[17] Yao L, Alderliesten RC, Benedictus R. The effect of fibre bridging on the Paris relation for mode I fatigue delamination growth in composites. Compos Struct 2016;140:125–35.
[18] Albertsen H, Ivens J, Peters P, Wevers M, Verpoest I. Interlaminar fracture toughness of CFRP influenced by fibre surface treatment: Part 1 Experimental results. Compos Sci Technol 1995;54(2):133–45.
[19] Sorensen L, Botsis J, Gmür Th, Humbert L. Bridging tractions in mode I delamination: Measurements and simulations. Compos Sci Technol 2008;68(12):2350–8.
[20] Sorensen L, Botsis J, Gmür T, Cugnoni J. Delamination detection and characterisation of bridging tractions using long FBG optical sensors. Compos Part A Appl Sci Manuf 2007;38(10):2087–96.
[21] Herráez M, Pichler N, Botsis J. Improving delamination resistance through tailored defects. Compos Struct 2020;247:112422.
[22] Kachanov M, Montagut ELE, Laures JP. Mechanics of crack—microcrack interactions. Mech Mater 1990;10(1–2):59–71.
[23] Brunner AJ, Blackman BRK, Williams JG. Calculating a damage parameter and bridging stress from GIC delamination tests on fibre composites. Compos Sci Technol 2006;66(6):785–95.
[24] Modi D, Comer A, O'Higgins RMO, McCarthy MA. Thermoplastic composites: in-situ consolidation or in-situ welding. In: Proceedings of the 19th international conference on composite materials (ICCM 19), 2013; Montreal, Canada.
[25] Qureshi Z, Swait T, Scaife R, El-Dessouky HM. In situ consolidation of thermoplastic prepreg tape using automated tape placement technology: Potential and possibilities. Compos B Eng 2014;66:255–67.
[26] Bandaru AK, Clancy GJ, Peeters D, O'Higgins R, Weaver PM. Interface characterization of thermoplastic skin-stiffener composite manufactured using laser-assisted tape placement. In: 2018 AIAA/ASCE/AHS/ASC Structures, Structural Dynamics, and Materials Conference, 2018, p. 0481.
[27] Barnes JA, Byerly GE. The formation of residual stresses in laminated thermoplastic composites. Compos Sci Technol 1994;51(4):479–94.
[28] Mei Z, Chung DDL. Effect of heating time below the melting temperature on polyphenylene sulfide adhesive joint development. Int J Adhes Adhes 2000;20(4):273–7.
[29] Ghadirdokht A, Heidari-Rarani M. Delamination R-curve behavior of curved composite laminates. Compos B Eng 2019;175:107139.
[30] Yokozeki T, Ogasawara T, Aoki T. Correction method for evaluation of interfacial fracture toughness of DCB, ENF and MMB specimens with residual thermal stresses. Compos Sci Technol 2008;68(3–4):760–7.
[31] ASTM D790 Standard test methods for flexural properties of unreinforced and reinforced plastics and electrical insulating materials.
[32] Yee RY, Stephens TS. A TGA technique for determining graphite fiber content in epoxy composites. Thermochim Acta 1996;272:191–9.
[33] Brunner AJ, Blackman BRK, Williams JG. Deducing Bridging Stresses and Damage from GIC Tests on Fibre Composites. In: Blackman BRK, Pavan A, Williams JG, editors. Fracture of polymers, composites, and adhesives II. Amsterdam, Boston: Elsevier; 2003. p. 479–90.
[34] Brunner AJ, Murphy N, Pinter G. Development of a standardized procedure for the characterization of interlaminar delamination propagation in advanced composites under fatigue mode I loading conditions. Eng Fract Mech 2009;76(18):2678–89.
[35] De Morais AB, Pereira AB. Application of the effective crack method to mode I and mode II interlaminar fracture of carbon/epoxy unidirectional laminates. Compos Part A Appl Sci Manuf 2007;38(3):785–94.
[36] Williams JG, Hadavinia H, Cotterell B. Anisotropic elastic and elastic–plastic bending solutions for edge constrained beams. Int J Solids Struct 2000;42(18–19):4927–46.
[37] Liu D, Zhu Y, Ding J, Lin X, Fan X. Experimental investigation of carbon fiber reinforced poly(phenylene sulfide) composites prepared using a double-belt press. Compos B Eng 2015;77:363–70.
[38] Brunner AJ. Fracture mechanics test standards for fiber-reinforced polymer composites: Suggestions for adapting them to Industry 4.0 and the digital age. Procedia Struct Integrity 2020;28:546–54.
[39] Pascoe JA, Rans CD, Benedictus R. Characterizing fatigue delamination growth behaviour using specimens with multiple delaminations: The effect of unequal delamination lengths. Eng Fract Mech 2013;109:150–60.
[40] Choi NS, Kinloch AJ, Williams JG. Delamination Fracture of Multidirectional Carbon-Fiber/Epoxy Composites under Mode I, Mode II and Mixed-Mode I/II Loading. J Compos Mater 1999;33(1):73–100.
[41] Davies P, Cantwell W, Moulin C, Kausch HH. A study of the delamination resistance of IM6/PEEK composites. Compos Sci Technol 1989;36(2):153–66.
[42] Yao L, Alderliesten R, Zhao M, Benedictus R. Bridging effect on mode I fatigue delamination behavior in composite laminates. Compos Part A Appl Sci Manuf 2014;63:103–9.